Journal of Organometallic Chemistry 703 (2012) 25–33

Contents lists available at SciVerse ScienceDirect

Journal of Organometallic Chemistry

journal homepage: www.elsevier.com/locate/jorganchem

Infrared spectra and density functional calculations of the M←NCCCH$_3$, η^2–M(NC)–CH$_3$, CH$_3$–MNC, CH$_2$=M(H)NC, and CH≡M(H)$_2$NC complexes produced by reactions of Group 6 metal atoms with acetonitrile

Han-Gook Cho [a,b], Lester Andrews [a,b,*]

[a] Department of Chemistry, University of Incheon, 119 Academy-ro, Yonsu-gu, Incheon 406-772, South Korea
[b] Department of Chemistry, University of Virginia, P.O. Box 400319, Charlottesville, VA 22904-4319, USA

ARTICLE INFO

Article history:
Received 10 November 2011
Received in revised form
5 December 2011
Accepted 6 December 2011

Keywords:
Matrix infrared spectra
DFT calculations of frequencies and structures
Cr, Mo, W
Acetonitrile reaction products

ABSTRACT

The M←NCCH$_3$, η^2–M(NC)–CH$_3$, CH$_3$–MNC, CH$_2$=M(H)NC, and HC≡M(H)$_2$NC complexes are produced by reactions of laser-ablated Group 6 metal atoms with acetonitrile and identified from the matrix IR spectra through isotopic substitution and comparison to frequencies calculated by density functional theory in the harmonic approximation (B3LYP/6-311++(3df,3pd) and BPW91/6-311++G(3df,3pd), this all-electron set for Cr, and SDD for Mo and W). Good general agreement is shown in tables for all observed frequencies and these calculations. The products follow the reaction path proposed earlier for Group 4 and 5 metal reactions, which are supported by density functional energy calculations. The M←NCCH$_3$ complex strengthens the assumption that the lone electron pair on the N-end first attracts the metal atom. The π-complexes show that the back-donation of the Group 6 metal is weaker than those of Zr and Group 5 metals. The observed products clearly show the increasing preference for the higher oxidation-state complex with increasing atomic number of the Group 6 metal, and subsequent photolysis increases the yields for the higher oxidation-state complexes. The methylidyne isocyanide HC≡W(H)$_2$NC has a C$_s$ structure similar to the HC≡W(H)$_2$X complexes prepared earlier.

1. Introduction

Acetonitrile has been a model compound in the development of vibrational spectroscopy due to its relatively simple spectra from the C$_{3v}$ structure and coincidence with the CO$_2$ laser lines [1]. Its C–N stretching band, which is located in a relatively clean area, has also been the subject of many spectroscopic studies, particularly because it is a useful probe for examining the coordination strength with its N-end to electron-deficient species [2]. The lone electron pair on the N-end provides substantial anti-bonding character in the molecular axis, particularly in the CN bond, which often leads to blue shifts of the stretching bands upon coordination to an acceptor particularly in solution [3]. The photochemical reactions of acetonitrile, such as conversions between CH$_3$CN and CH$_3$NC, have also drawn much attention [4]. Acetonitrile isomers and fragments, such as H$_2$CCNH, HCNCH$_2$, and HCNC, have also been prepared from photo-dissociation of larger precursors [5].

A series of studies have shown that reactions of transition-metals with small hydrocarbons and their halides are efficient routes to produce new breed of small characteristic complexes, including carbenes, carbynes, π-complexes, and cyclic products via C–H(X) bond insertion and H(X) migration from C to M [6–11]. Because of their relatively small number of atoms, they are also more amenable to high level theoretical approaches to provide helpful information for spectral assignments and understanding the reaction mechanism [12]. They also allow opportunities to closely monitor molecular processes involved in metal coordination, bond insertion, H(X) migration, and their photochemical behaviors. These results show that C–H(X) bond insertion by transition-metals and subsequent reactions are in fact a general chemical phenomenon and can also be extended to other organic species [6–12].

Recently reactions of Zr and Group 5 metals with CH$_3$CN have been investigated in this laboratory [13,14]. The nitrile η^2–π-complex and isocyanide products (CH$_3$–ZrNC and CH$_2$=Zr(H)NC) result from reactions of Zr with acetonitrile without a trace of the cyanide complexes, leading to the proposal of reaction path (1) [13]. This path was later corroborated by the products formed in Group 5 metal reactions with acetonitrile, namely η^2–V(NC)–CH$_3$

---

[*] Corresponding author. Department of Chemistry, University of Virginia, P.O. Box 400319, Charlottesville, VA 22904-4319, USA.
E-mail address: lsa@virginia.edu (L. Andrews).

0022-328X/$ – see front matter © 2012 Elsevier B.V. All rights reserved.
doi:10.1016/j.jorganchem.2011.12.007

produced from V reactions and $CH_3{-}VNC$ in subsequent photolysis, $CH_3{-}NbNC$ and $\eta^2{-}Nb(NC){-}CH_3$ from Nb reactions and $CH_2{=}Nb(H)NC$ during photolysis, and $CH_2{=}Ta(H)NC$ from Ta reactions [14].

$$\begin{aligned} &M + CH_3CN \rightarrow M \leftarrow NCCH_3 \rightarrow \eta^2{-}M(NC){-}CH_3 \\ &\quad \rightarrow CH_3{-}MNC \rightarrow CH_2{=}M(H)NC \rightarrow HC{\equiv}M(H)_2NC \end{aligned} \qquad (1)$$

In metal atom reactions with CH_3CN, the electron-rich N-end of acetonitrile is expected to initially attract the electron-deficient metal atom, as it does on solvation or on forming acetonitrile adducts [2,3]. However, the coordination complex ($M \leftarrow NCCH_3$) was not identified in the matrix spectra probably due to its relatively higher energy and rapid conversion to the nitrile $\eta^2{-}\pi$-complex.

In this investigation, reactions of Group 6 metals with acetonitrile isotopomers are carried out and the results are compared with the previous Zr and Group 5 metal results [13,14]. The primary products are identified through isotopic substitution and with helpful information from DFT computations. The observed products are the five constituents of reaction path (1) while showing increasing preference for the higher oxidation-state product with increasing atomic number of the Group 6 metal.

2. Experimental and computational methods

Laser-ablated Cr, Mo, and W atoms were reacted with acetonitrile isotopomers (CH_3CN, CD_3CN, and $^{13}CH_3{}^{13}CN$) in excess argon during condensation at 10 K using a closed-cycle refrigerator (Air Products Displex). These methods have been described in detail in previous publications [6a,15]. Reagent gas mixtures are typically 0.5% in argon. The Nd:YAG laser fundamental (1064 nm, 10 Hz repetition rate, 10 ns pulse width) was focused onto a rotating metal target (Johnson-Matthey) using 5–10 mJ/pulse. After initial reaction, infrared spectra were recorded at 0.5 cm^{-1} resolution using a Nicolet 550 spectrometer with a liquid nitrogen cooled Hg–Cd–Te range B detector. Then samples were irradiated for 20 min periods by a mercury arc street lamp (Sylvania, 175 W) with the globe removed using a combination of optical filters or annealed to allow further reagent diffusion.

In order to provide support for the assignment of new experimental frequencies and to correlate with previous related works [6–11], density functional theory (DFT) calculations were performed in the harmonic approximation using the Gaussian 09 package [16a], the B3LYP density functional [17], the 6-311++G(3df,3pd) basis sets for H, C, N, and Cr [18] and the SDD pseudopotential and basis sets [19] for Mo and W to provide vibrational frequencies for prospective reaction products. We find the all-electron DZVP set [16b,c] to give higher frequencies than the above sets for Mo as a test case, which are thus further above the observed frequencies. Geometries were fully relaxed during optimization, and the optimized geometries were confirmed by vibrational analysis. The BPW91 and M06 functionals [20] were also employed to complement the B3LYP results. The vibrational frequencies were calculated analytically, and zero-point energy is included in the calculation of binding and reaction energies. Previous investigations have shown that DFT calculated harmonic frequencies are usually slightly higher than observed frequencies [6–11,21], but they correlate well and provide useful predictions and support for assigning the infrared spectra of new molecules.

3. Results and discussion

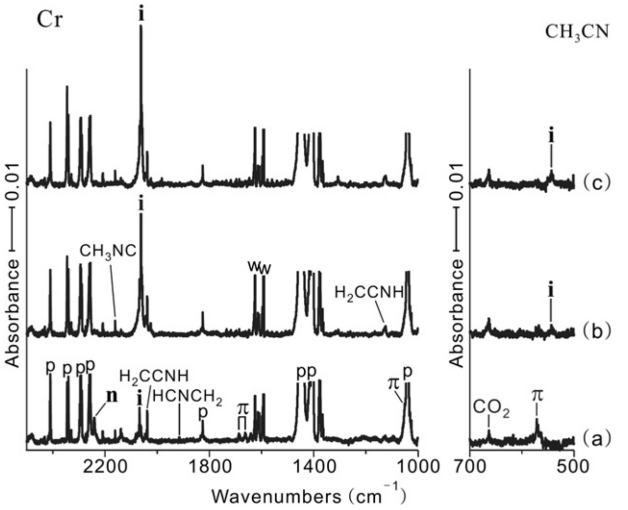

Fig. 1. Infrared spectra from reaction products of laser-ablated chromium with CH_3CN in excess argon at 10 K. (a) Cr and CH_3CN (0.50% in argon) co-deposited for 1 h, (b) as (a) after visible ($\lambda > 420$ nm) and UV (240–380 nm) irradiation and (c) as (b) after full arc ($\lambda > 220$ nm) photolysis. Relatively small intensity changes are observed on visible irradiation and the product absorptions gradually decrease on annealing (see text). **n**, π, and **i** designate the product absorption groups while P and c stand for the precursor and common absorptions in the CH_3CN matrix spectra. H_2CCNH, $HCNCH_2$, and CH_3NC absorptions are also indicated.

Reactions of Group 6 metal atoms with acetonitrile were investigated and infrared spectra (Figs. 1–6 and S1–S3, and Tables 1–3) and density functional frequency calculations of the products (Tables S1–S15) and their relative energies (Figs. 7–9) and structures (Figs. 10–12) will be presented in turn.

3.1. Cr + acetonitrile

The first figures illustrate product spectra from reactions of laser-ablated Cr atoms with acetonitrile isotopic modifications and show their variation on subsequent sample photolysis and annealing. The isomerization products of acetonitrile (CH_2CNH, CH_2NCH, and CH_3NC) [4,5], due to the laser-plume radiation during ablation [6a,15] are also observed, but these absorptions are weak relative to those in previous studies [4,5], and the Mo and W cases described below. Here three sets of new product absorptions are marked **n**, π, and **i** (for **N**-coordination, π-, and insertion

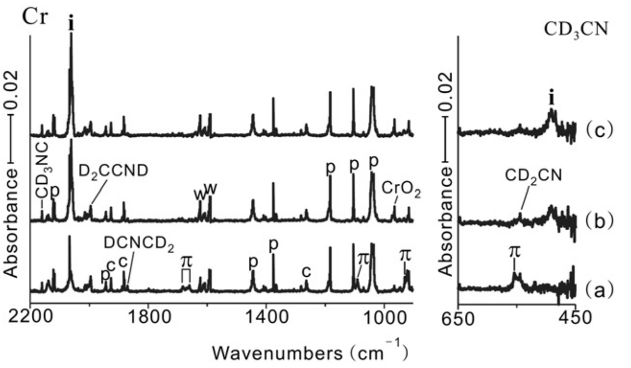

Fig. 2. Infrared spectra from reaction products of laser-ablated chromium with CD_3CN in excess argon at 10 K. (a) Cr and CD_3CN (0.50% in argon) co-deposited for 1 h, (b) as (a) after visible ($\lambda > 420$ nm) and UV (240–380 nm) irradiation, and (c) as (b) after full arc ($\lambda > 220$ nm) photolysis. Relatively small intensity changes are observed on visible irradiation and the product absorptions gradually decrease on annealing (see text). **n**, π, and **i** stand for the product absorption groups while P and c designate the precursor and common absorptions in the CD_3CN matrix spectra. D_2CCND, $DCNCD_2$, and CD_3NC absorptions are also indicated. Bands labeled c are common for this precursor and different metals.

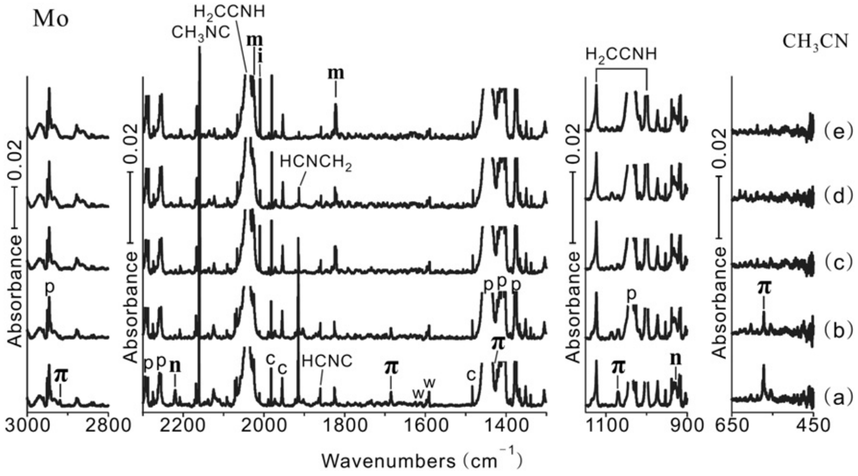

Fig. 3. Infrared spectra from reaction products of laser-ablated molybdenum with CH_3CN in excess argon at 10 K. (a) Mo and CH_3CN (0.50% in argon) co-deposited for 1 h, (b) as (a) after visible ($\lambda > 420$ nm) irradiation, (c) as (b) after UV (240–380 nm) irradiation, (d) as (c) after visible irradiation, and (e) as (d) after UV irradiation. The product absorptions gradually decrease on annealing (see text). π, **i**, and **m** stand for the product absorption groups while P and c designate the precursor and common absorptions in the CH_3CN matrix spectra. H_2CCNH, $HCNCH_2$, CH_3NC, and HCNC absorptions are also indicated. Bands labeled c are common for this precursor and different metals.

complexes) on the basis of intensity variation during photolysis and annealing of the deposited samples.

The **n** absorption decreases slightly on visible ($\lambda > 420$ nm) irradiation, and almost disappears on the following UV (240–380 nm) irradiation. The π absorptions decrease to about a third of their original intensity on visible irradiation and almost disappear on UV irradiation. On the other hand, the **i** absorptions remain unchanged on visible irradiation, more than triple on UV irradiation, further increase on full arc ($\lambda > 220$ nm) photolysis, and decrease on annealing. The observed frequencies are listed in Table 1 and compared with the DFT computed values in Tables S1–S5 for plausible reaction products.

The **n** absorption observed at 2240.8 cm^{-1} has a D counterpart 2040 cm^{-1} shoulder band and a ^{13}C counterpart at 2188.9 cm^{-1} (carbon 12/13 frequency ratio of 1.024). It most probably originates from a C–N stretching mode on the basis of its frequency position and large ^{13}C shift. However, its frequency is substantially higher than those of the previously studied cyanide and isocyanide complexes, which are expected in the 2150–2050 cm^{-1} region. Other possible cyanide or isocyanide products, such as CrNC and CrCN, would not show N–C and C–N stretching bands in this high frequency region. In fact, the observed frequency is close to the C–N stretching frequency of 2258 cm^{-1} for CH_3CN [13,14,22]. We attribute this photosensitive band to the C–N stretching mode of the N-coordinated complex [2,3], $Cr \leftarrow NCCH_3$, on the basis of good correlation with the computed values (B3LYP, Table S1, 2297.0 cm^{-1} and ^{13}C shift of 56.1 cm^{-1}).

The observed C–N stretching band is the strongest one we calculated for the N-coordinated complex with a bent Cr–N–C–C backbone, and all other bands are too weak to observe, as shown in Table S1. Unfortunately, the B3LYP calculation gave a small 31 cm^{-1} imaginary CrNC bending frequency with B3LYP/6-311++(3df,3pd), which was even larger (−38 cm^{-1}) with B3LYP/DZVP [16]. Many attempts with different initial structures failed to remove this small imaginary frequency, which arises with the B3LYP functional. Although BPW91/6-311++G(3df,3pd) gave a real 24 cm^{-1} CrNC bending frequency, the calculated C–N stretch was 88 cm^{-1} lower than the observed value. However, the ab initio MP2 method [16c] computed a linear complex, a real 47 cm^{-1} CrNC bending frequency, and a much higher value (2431 cm^{-1}) for the observed C–N stretch. This latter value shows the usual relationship between

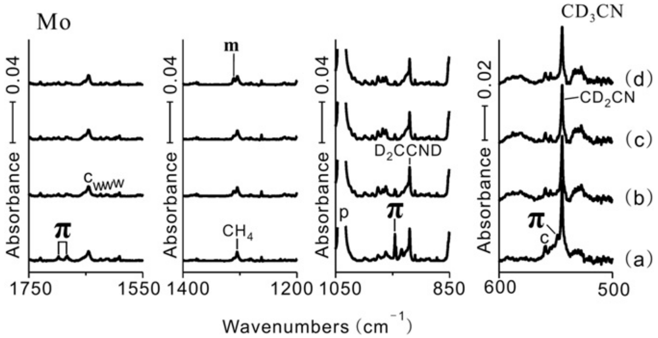

Fig. 4. Infrared spectra from reaction products of laser-ablated molybdenum with CD_3CN in excess argon at 10 K. (a) Mo and CD_3CN (0.50% in argon) co-deposited for 1 h, (b) as (a) after visible ($\lambda > 420$ nm) and UV (240–380 nm) irradiation, (c) as (b) after visible irradiation, and (d) as (c) after UV irradiation. Relatively small intensity changes are observed on the first visible irradiation and the product absorptions gradually decrease on annealing (see text). π, **i**, and **m** stand for the product absorption groups while P and c designate the precursor and common absorptions in the CD_3CN matrix spectra. D_2CCND, $DCNCD_2$, and CD_3NC absorptions are also indicated. Bands labeled c are common for this precursor and different metals.

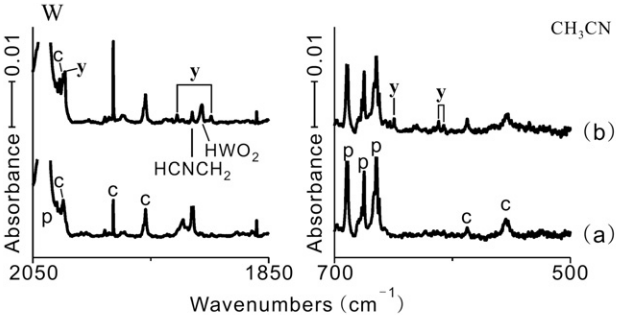

Fig. 5. Infrared spectra from reaction products of laser-ablated tungsten with CH_3CN in excess argon at 10 K. (a) W and CH_3CN (0.50% in argon) co-deposited for 1 h and (b) as (a) after visible ($\lambda > 420$ nm) and UV (240–380 nm) irradiation. Relatively small intensity changes are observed on visible irradiation and the product absorptions gradually decrease on annealing (see text). y stands for the product absorption while P and c designate the precursor and common absorptions in the CH_3CN matrix spectra. $HCNCH_2$ and HWO_2 absorptions are also indicated. Bands labeled c are common for this precursor and different metals.

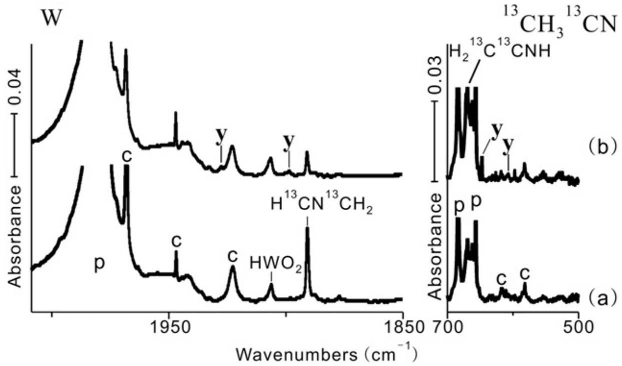

Fig. 6. Infrared spectra from reaction products of the laser-ablated tungsten with $^{13}CH_3{}^{13}CN$ in excess argon at 10 K. (a) W and $^{13}CH_3{}^{13}CN$ (0.50% in argon) co-deposited for 1 h and (b) as (a) after visible ($\lambda > 420$ nm) and UV (240–380 nm) irradiation. Relatively small intensity changes are observed on visible irradiation and the product absorptions gradually decrease on annealing (see text). **y** stands for the product absorptions while p and c designate the precursor and common absorptions in the $^{13}CH_3{}^{13}CN$ matrix spectra. $H_2^{13}C^{13}CNH$ and $H^{13}CN^{13}CH_2$ absorptions are also indicated. Bands labeled c are common for this precursor and different metals.

MP2 and B3LYP frequencies [21] and suggests that the small 31 cm^{-1} imaginary CrNC bending frequency with B3LYP does not invalidate the higher calculated frequencies (Table S1). We also give the computed Cartesian coordinates using B3LYP for the structures in each table.

We believe that this is the first observation of an acetonitrile N-coordination complex with a metal atom in matrix isolation spectra. The N-coordinated complexes with metal cations are commonly discovered in acetonitrile adducts, which explain the solution spectra of various salts [2,3]. Coordination with its N-end alleviates the anti-bonding character supplied from the lone electron pair and thus, leads to only a small red shift and sometimes even a blue shift particularly in solution.

A strong **π** absorption is observed at 571.4 cm^{-1} along with its D and ^{13}C counterparts at 554.1 and 568.0 cm^{-1}. Among the plausible products, only the π-complex (η^2–Cr(NC)–CH_3) has such a strong absorption (the N–Cr stretching band) in the low frequency region [13,14]. The observed frequencies are between the B3LYP values of 567.8, 550.9, and 565.2 cm^{-1} and the BPW91 values of 581.8, 568.4, and 579.2 cm^{-1} (Table S2). The other π absorptions also support generation of η^2–Cr(NC)–CH_3. The strong **π** absorption at 1050.6 cm^{-1} on the shoulder of a precursor band shifts to 922.0 cm^{-1} on deuteration. While the ^{13}C counterpart is believed to be covered by precursor absorption, it is designated to the CH_3 rocking mode. The **π** absorption at 1434.9 cm^{-1} [shoulder, requires expanded spectra for clear observation] is accompanied with D and ^{13}C counterparts at 1090.7 and 1432.1 cm^{-1}, and assigned to the CH_3 bending mode. Another **π** absorption at 1685.9 cm^{-1} shifts to 1683.5 and 1647.0 cm^{-1} on D and ^{13}C substitution and is assigned to the CCN anti-symmetric stretching mode on the basis of the small D and large ^{13}C shifts. In the high frequency region, the **π** absorption at 2912.7 cm^{-1} along with its ^{13}C counterpart at 2909.1 cm^{-1} is designated to the CH_3 symmetric stretching mode. The observed five absorptions substantiate generation of the nitrile π-complex [23].

Table 1
Vibrational frequencies of product absorptions observed from reactions of Cr with acetonitrile isotopomers in excess argon.[a]

	CH_3CN	CD_3CN	$^{13}CH_3{}^{13}CN$	Description
N	2240.8	2240 sh	2188.9	A_1 C–N str.
Π	2912.7	Covered	2909.1	A′ CH_3 s. str.
	1685.9	1683.5	1647.0	A′ CCN as. str.
	1434.9	1090.7	1432.1	A′ CH_3 bend
	1050.6	922.0	Covered	A′ CH_3 rock
	571.4	554.1	568.0	A′ Cr–N str.
i	2061.6	2061.4	2021.0	A′ N–C str.
	550.6	483.9	546.3	A′ C–Cr str.
		491.0	511.9	A′ Cr–N str.

[a] All frequencies are in cm^{-1}. Description gives major vibrational coordinate.

Table 2
Vibrational frequencies of product absorptions observed from reactions of Mo with acetonitrile isotopomers in excess argon.[a]

	CH_3CN	CD_3CN	$^{13}C_3^{13}CN$	Description
N	2220.0	Covered	2167.5	A_1 C–N str.
	928.5		906.4	A_1 C–C str.
Π	2919.1	2107.5	1915.4	A′ CH_3 s. str.
	1684.5	1697.7, **1682.7**	1644.5	A′ CCN as. str.
	1436.0	Covered	1432.8	A′ CH_3 bend
	1071.5, 1068.2	**945.9**, 944.1	1048	A′ CH_3 rock
	574.1, **571.7**	548.5	570.0, **567.1**	A′ Mo–N str.
i	2010.9	2010.2	1971.4	A′ N–C str.
m	2029.2, 2026.7	2029.3, 2026.6	1986.3	A′ N–C str.
	1823.6, 1821.7	1311.7, 1310.5	1823.2, 1821.7	A′ Mo–N str.
	823.9			A′ C–Mo str.

[a] All frequencies are in cm^{-1}. Stronger matrix site absorptions in a set are bold. Description gives major coordinate.

The strongest product absorption (marked "**i**") is observed at 2061.6 cm^{-1} with D and ^{13}C counterparts at 2061.4 and 2021.0 cm^{-1}. We assign the uniquely strong **i** absorption to the N–C stretching mode of CH_3–CrNC on the basis of its frequency and good correlation with the DFT values (Table S3), parallel to the Zr and Group 5 metal cases [13,14]. The observed frequencies and D and ^{13}C isotopic shifts are compared with the B3LYP values of 2114.0 and 0.1 and 42.2 cm^{-1} (Table S3). A weak **i** absorption assigned to the C–Cr stretching mode is observed at 550.6 cm^{-1} in the low frequency region along with its D and ^{13}C counterparts at 483.9 and 546.3 cm^{-1}. Another **i** absorption at 491.0 cm^{-1} in the CD_3CN spectra is designated to the Cr–N stretching mode with the ^{13}C counterpart at 511.9 cm^{-1}. The observed absorptions substantiate formation of the insertion complex. The insertion complex is also the most stable among the plausible Cr products in the proposed reaction. The Cr←$NCCH_3$, η^2–Cr(NC)–CH_3, CH_3–CrNC, CH_2═Cr(H)NC, and HC≡Cr(H)$_2$NC reaction products in their septet, quintet, quintet, triplet, and singlet ground states are −22, −4, −62, +125, and +302 kJ/mol (B3LYP values) with respect to the reactants (Cr(^7S) + CH_3CN), respectively. Thus, we only observe the products with energies lower than reactants.

3.2. Mo + acetonitrile

The product absorptions from molybdenum atom reactions with CH_3CN isotopomers are displayed in Figs. 3 and 4, and S2. Unlike the Cr case, the Mo ablation plume [15] yields strong acetonitrile isomerization product absorptions (H_2CCNH, $HCNCH_2$ [5], CH_3NC [4], and HCNC [24]). Four groups of product absorptions

Table 3
Vibrational frequencies of product absorptions observed from reactions of W with acetonitrile isotopomers in excess argon.[a]

	CH_3CN	CD_3CN	$^{13}CH_3{}^{13}CN$	Description
y	2023.0	2023.1	1984.4	A′ N–C str.
	1927.5	Covered	1927.4	A′ WH_2 s. str.
	1898.7	1354.9	1898.3	A″ WH_2 as str.
	649.5		647.4	A′ WH_2 wag
	611.7, **607.4**		607.0	A″ WH_2 twist

[a] All frequencies are in cm^{-1}. Stronger absorptions in a set are bold. Description gives major vibrational coordinate.

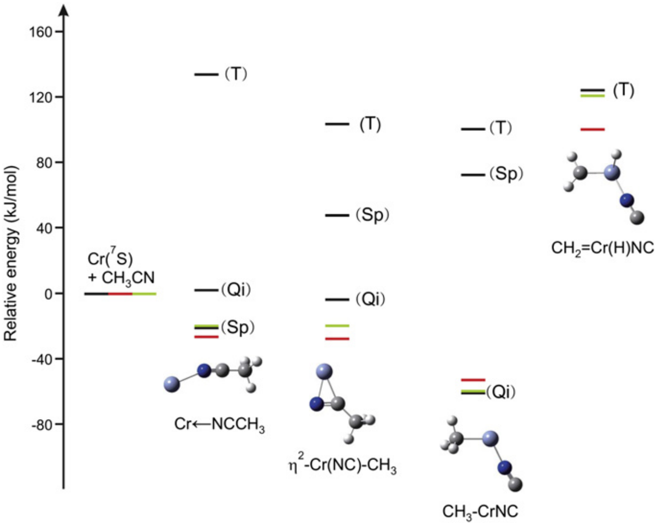

Fig. 7. Electronic energies (ZPE correction included) for the plausible Cr products in the proposed reaction path (1) relative to the reactants (Cr(^{7}S) + CH_3CN). Black lines denote B3LYP energies for several electronic states of each product, but only the ground state for the methylidene: Red lines denote BPW91 and green lines indicate M06 energies for the ground state structure of each product. Only Cr ← $NCCH_3$, η^2—Cr(NC)—CH_3, CH_3—CrNC are observed in the matrix IR spectra. In the process of photolysis, the Cr ← $NCCH_3$ and Cr—η^2—(NC)—CH_3, absorptions decrease while those of CH_3—CrNC increase, corroborating the reaction path. CH_2═Cr(H)NC is not observed probably due to its high energy (see text). T indicates triplet, Qi denotes quintet, and Sp indicates septet states. (For interpretation of the references to colour in this figure legend, the reader is referred to the web version of this article.)

marked "**n**, π, **i**, and **m**" (**m** for **m**ethylidene) are observed and grouped depending on intensity changes upon photolysis and annealing. The **n** absorptions decrease to less than a fifth of their original intensity on the first visible irradiation, remain unchanged on the next UV irradiation, and completely disappear on the second visible photolysis. Similar to the Cr case, the π absorptions decrease ~50% on visible photolysis and almost disappear on UV irradiation. The **i** and **m** absorptions show reversible intensity changes during photolysis. They decrease on visible irradiation but increase on UV photolysis repeatedly as shown in Figs. 3 and 4, and S2. The **i** absorptions, however, show more dramatic intensity variation, for example, becoming 8 times as strong on the first UV irradiation and decreasing to a third in intensity on the second visible irradiation.

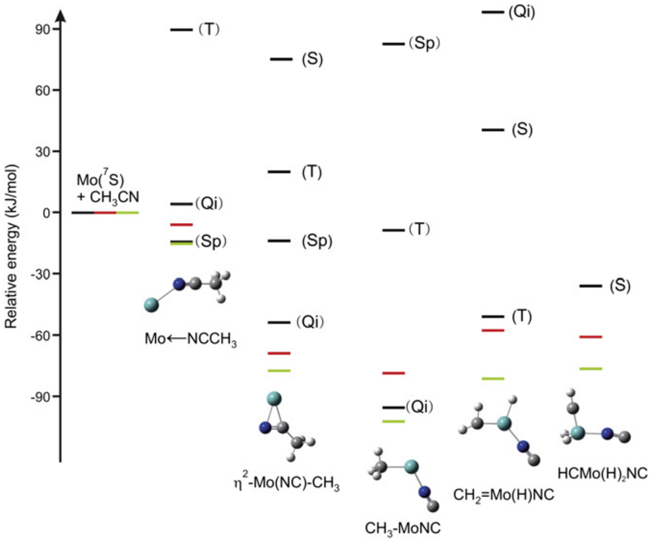

Fig. 8. Electronic energies (ZPE correction included) for the plausible Mo products in the proposed reaction path (1) relative to the reactants (Mo(^{7}S) + CH_3CN). Black lines denote B3LYP energies for several electronic states of each product, but only the ground state for the methylidyne: Red lines denote BPW91 and green lines indicate M06 energies for the ground state structure of each product. Energies of the plausible Mo products in the proposed reaction path (1) relative to the reactants (Mo(^{7}S) + CH_3CN). Mo ← $NCCH_3$, η^2—Mo(NC)—CH_3, CH_3—MoNC and CH_2═Mo(H)NC are observed in the original matrix IR spectra. The insertion and methylidene product absorptions increase on UV irradiation but decrease on visible increase in concert. HC≡Mo$(H)_2$NC is not observed probably due to its high energy. T indicates triplet, Qi denotes quintet, and Sp indicates septet states. (For interpretation of the references to colour in this figure legend, the reader is referred to the web version of this article.)

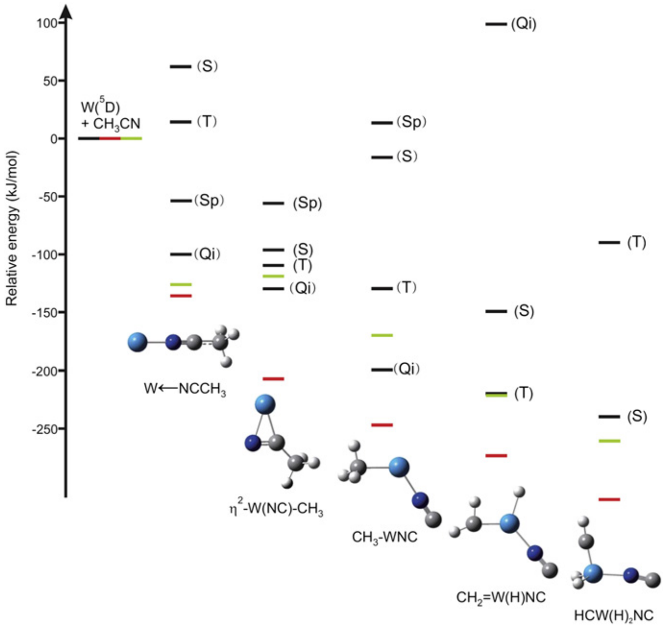

Fig. 9. Electronic energies (ZPE correction included) for the plausible W products in the proposed reaction path (1) relative to the reactants (W(^{5}D) + CH_3CN). Black lines denote B3LYP energies for several electronic states of each product: Red lines denote BPW91 and green lines indicate M06 energies for the ground state structure of each product. Energies of the plausible W products in the proposed reaction path (1) relative to the reactants (W(^{5}D) + CH_3CN). Only HC≡W$(H)_2$NC, the most stable product, is observed. The methylidyne product absorptions increase on UV irradiation. T indicates triplet, Qi denotes quintet, and Sp indicates septet states. (For interpretation of the references to colour in this figure legend, the reader is referred to the web version of this article.)

A stronger **n** absorption is observed at 2220.0 cm^{-1}, and its ^{13}C counterpart at 2167.5 cm^{-1}. Following the Cr case, where the corresponding **n** absorption is observed at 2240.8 cm^{-1}, this band is assigned to the C—N stretching mode of the N-coordinated complex (Mo ← $NCCH_3$), while the D counterpart is not observed in the congested precursor band area. The observed frequency and ^{13}C shift correlate well with the B3LYP values of 2290.4 and 56.2 cm^{-1}. Another **n** absorption and its ^{13}C counterpart are observed at 928.5 and 906 cm^{-1} and are appropriate for the C—C stretching mode (Table S6). The N-coordinated complexes in both the Cr and Mo systems provide evidence for the initial coordination of acetonitrile with its N-end to the metal atom.

The strongest π absorption is observed at 571.7 cm^{-1} (with a site absorption at 574.1 cm^{-1}) and its D and ^{13}C counterparts at 548.5 and 567.1 cm^{-1} (H/D and 12/13 ratios of 1.042 and 1.008). Parallel to the Cr case, only the π-complex among the plausible products has its strongest band in the low frequency region, and it is assigned to the Mo—N stretching mode of η^2—Mo(NC)—CH_3. Other π absorptions all support formation of the π-complex as well. The π absorptions at 1436.0 and 1071.5 cm^{-1} are assigned to the CH_3 bending and rocking modes on the basis of their frequencies and isotopic (large D and small ^{13}C) shifts (Tables 2 and S7). The π absorption at 1684.5 cm^{-1} holds its D and ^{13}C counterpart at 1682.7

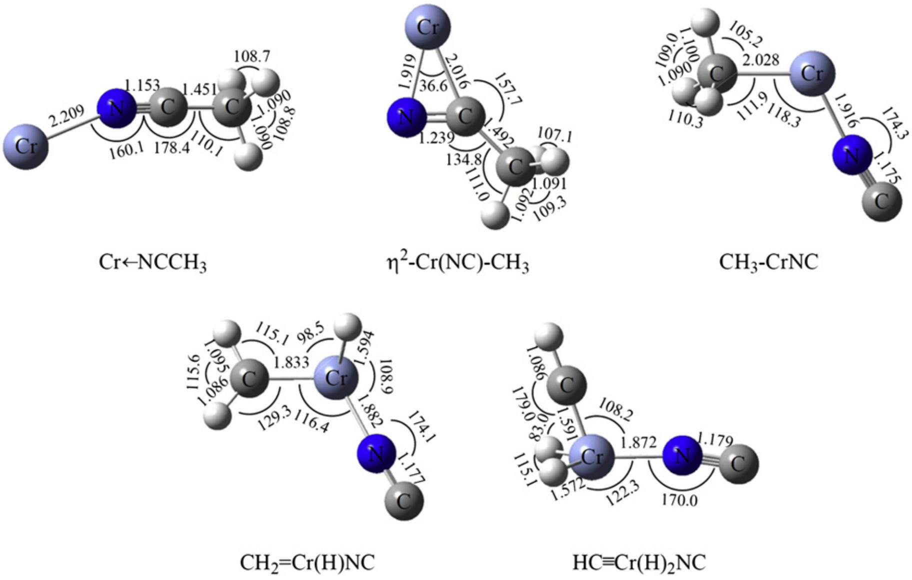

Fig. 10. The B3LYP structures of several Cr products using the 6-311++G(3df,3pd) basis sets for H, C, N, and Cr. Bond distances and angles are in Å and deg. The Cr←NCCH$_3$ complex has a septet ground state, the Cr methylidene has a triplet ground state, whereas the others have quintet ground state. CH$_2$=Cr(H)NC has a C$_1$ structure.

and 1644.5 cm^{-1} (H/D and 12/13 ratios of 1.001 and 1.024) and is designated to the CCN anti-symmetric stretching mode. In the high frequency region, another π absorption at 2919.1 cm^{-1} is assigned to the CH$_3$ symmetric stretching mode with its D and ^{13}C counterparts at 2107.5 and 2915.4 cm^{-1} (H/D and 12/13 ratio of 1.385 and 1.001). The observed five absorptions and their isotopic counterparts substantiate production of the π-complex in reaction of Mo with acetonitrile, parallel to the Cr case.

A strong **i** absorption is observed at 2010.9 cm^{-1} and its D and ^{13}C counterparts at 2010.2 and 1971.4 cm^{-1} (H/D and 12/13 ratios of 1.000 and 1.020) with dramatic intensity variation during photolysis. We designate the **i** absorption to the N–C stretching mode of CH$_3$–MoNC while other **i** absorptions are too weak to observe. The observed frequency and isotopic shifts are consistent with the predicted frequency of 2077.6 cm^{-1} and the isotopic shifts of 0.1 and 41.8 cm^{-1} (Table S8). The insertion product has a uniquely strong N–C stretching band and other much weaker bands, and it is also the most stable among the plausible products. The Mo←NCCH$_3$, η^2–Mo(NC)–CH$_3$, CH$_3$–MoNC, CH$_2$=Mo(H)NC, and HC≡Mo(H)$_2$NC reaction products in the septet, quintet, quintet, triplet, and singlet ground states are 14, 55, 95, 54, and 36 kJ/mol lower in energy (B3LYP values) than the reactants (Mo(^{7}S) + CH$_3$CN), respectively.

A strong **m** absorption pair are observed at 1823.6 and 1821.7 cm^{-1} overlapped each other with similar intensities, and the D counterparts at 1311.7 and 1310.5 cm^{-1} (H/D ratio of both 1.390),

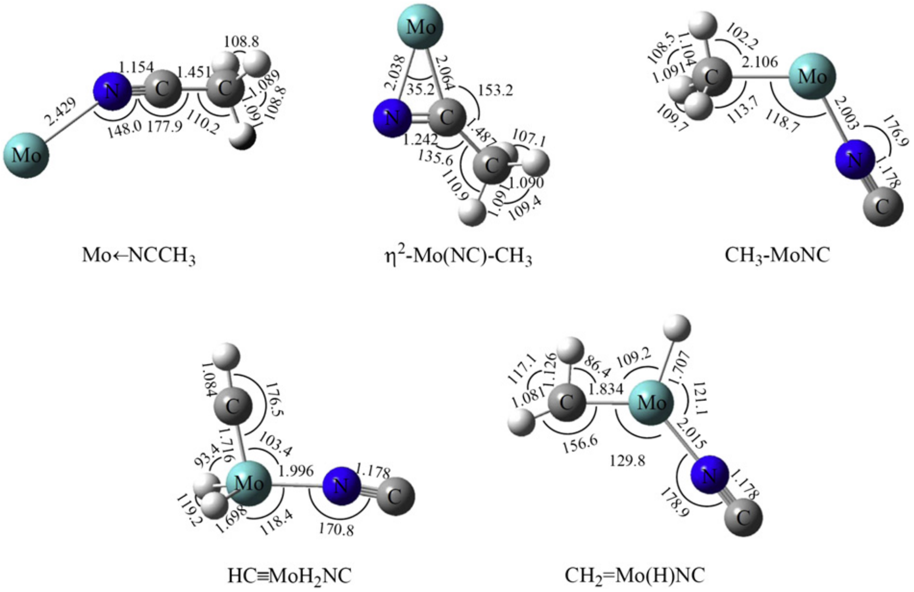

Fig. 11. The B3LYP structures of several Mo products using the 6-311++G(3df,3pd) basis sets for H, C, and N and SDD pseudo potential and basis for Mo. Bond distances and angles are in Å and deg. The Mo←NCCH$_3$ complex has a septet ground state, the Mo methylidene and methylidyne isocyanides have triplet and singlet ground states while the others have quintet grounds states. Notice the agostic distortion of the methylidene complex.

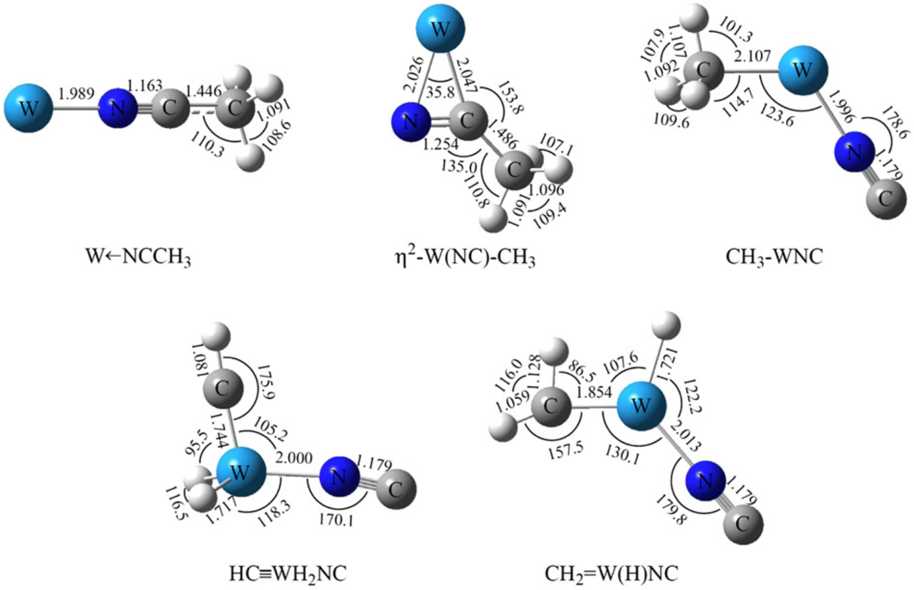

Fig. 12. The B3LYP structures of several W products using the 6-311++G(3df,3pd) basis sets for H, C, and N and SDD pseudo potential and basis for W. Bond distances and angles are in Å and deg. Parallel to the Cr and Mo cases, the W methylidene and methylidyne isocyanides have triplet and singlet ground states and the other complexes have quintet ground states.

and ^{13}C counterparts at 1823.2 and 1821.7 cm^{-1} (essentially no ^{13}C shifts). The large H/D ratio and negligible ^{13}C ratio reveal that a reaction product with an Mo–H bond is generated in the reaction of Mo with acetonitrile. The Mo–H stretching frequency is also compared with 1761.9 and 1718.7 cm^{-1} for MoH_2, 1812.1 cm^{-1} for MoH_4, 1857.6 cm^{-1} for MoH_6 [25], and 1791.6 and 1781.5 cm^{-1} for $CH_2{=}MoH_2$, 1839.7, 1836.4, 1830.0 cm^{-1} for $HC{\equiv}MoH_3$, 1797.7 cm^{-1} for $CH_2{=}Mo(H)F$, and 1849.7 and 1844.8 cm^{-1} for $HC{\equiv}Mo(H)_2F$ [6]. Another strong **m** absorption pair are observed at 2029.2 and 2026.7 cm^{-1}, and the D counterparts at 2029.3 and 2026.6 cm^{-1} and ^{13}C counterpart at 1986.3 cm^{-1}. We assign the observed **m** absorptions to the Mo–H and N–C stretching modes of $CH_2{=}Mo(H)NC$, a small metal containing conjugated system. A weak **m** absorption at 823.9 cm^{-1} is designated to the C–Mo stretching mode without observation of its D and ^{13}C counterparts.

The Mo methylidene complex is one of the most stable plausible products in the proposed reaction path (1). In the previously studied Mo + CH_4 system [6a], where both the methylidene and methylidyne products are observed, the $CH_2{=}MoH_2$ and $HC{\equiv}MoH_3$ in their triplet and singlet ground states are 50 and 46 kJ/mol higher than $CH_3{-}MoH$ in the quintet ground state. The Mo methylidyne ($HC{\equiv}Mo(H)_2NC$) is not observed in this study probably due to its higher energy. The identified complexes are the first four products of reaction path (1).

3.3. W + CH_3CN

Relatively weak product absorptions (all marked "**y**" for methylid**y**ne) are observed from reactions of W with acetonitrile and the ^{13}C-enriched reagent as shown in Figs. 5 and 6. They remain unchanged on visible irradiation, but double on UV irradiation. However, the acetonitrile isomerization product absorptions are as strong as in the Mo spectra. The **y** absorptions at 1927.5 and 1898.7 cm^{-1} show negligible ^{13}C shifts, but these absorptions are weak, and we do not observe the deuterium counterparts as deuteride transfer counterparts tend to be even weaker in these experiments [6a]. The W–H stretching frequency is compared with 1852.6 cm^{-1} for WH, 1866.2 cm^{-1} for WH_4, 1923.7 cm^{-1} for WH_6 [26], 1864.5 and 1817.2 cm^{-1} for $CH_2{=}WH_2$, 1896.3, 1893.1, and 1888.3 cm^{-1} for $HC{\equiv}WH_3$, and 1905.6 cm^{-1} for $CH_2{=}W(H)F$, and 1936.4 and 1930.4 cm^{-1} for $HC{\equiv}W(H)_2F$ [6].

The two W–H stretching absorptions suggest a primary product with a WH_2 group. Another **y** absorption at 2023.0 cm^{-1} on the side of a 2024.2 cm^{-1} common peak most likely originates from an isocyanide stretching motion as it shifts to 1984.4 cm^{-1} on ^{13}C substitution. We, therefore, tentatively assign these three absorptions to the N–C and WH_2 stretching modes of $HC{\equiv}W(H)_2NC$. The **y** absorptions at 649.5 and 607.4 cm^{-1} with ^{13}C counterparts at 647.4 and 607.0 cm^{-1} are assigned to the WH_2 wagging and twisting modes. The observed five **y** absorptions support the probable formation the tungsten methylidyne product (Table S15). No other possible product absorptions are observed in the W spectra.

The $HC{\equiv}W(H)_2NC$ product tentatively identified here would be the first transition-metal methylidyne prepared from acetonitrile, and unlike the Cr and Mo cases, the methylidyne for W, the last step in reaction path (1), is the most stable among the plausible products. $W{\leftarrow}NCCH_3$, $\eta^2{-}W(NC){-}CH_3$, $CH_3{-}WNC$, $CH_2{=}W(H)NC$, and $HC{\equiv}W(H)_2NC$ in their quintet, quintet, quintet, triplet, and singlet ground states are 99, 132, 199, 219, and 240 kJ/mol lower in energy (B3LYP values) than the reactants ($W(^5D)$ + CH_3CN), respectively.

3.4. Reactions

The new reaction products identified here (N-coordination, π-, and insertion complexes for Cr, the N-coordination, π-, insertion, and methylidene complexes for Mo, and the methylidyne complex for W) are the species that constitute reaction path (1). The tendency that the higher oxidation-state complex is more favored with moving down the group column is apparently the driving force to produce the final product (methylidyne complex) in the reaction of W. The trapped initial species (N-coordination and π-complexes) in the matrix from reaction of Cr and Mo also provide strong evidence for reaction path (1).

The energies of the products in reaction path (1) ($M{\leftarrow}NCCH_3$, $\eta^2{-}M(NC){-}CH_3$, $CH_3{-}MNC$, $CH_2{=}M(H)NC$, and $HC{\equiv}M(H)_2NC$) relative to the reactants in the Cr, Mo, and W systems, respectively, are illustrated in Figs. 7–9. The generation of $M{\leftarrow}NCCH_3$ and the isocyanide products reflects preferential initial binding of N to the metal atom, leading to the conversion of η^2–(NC)–CH_3 to CH_3–MNC rather than to the C–C bond insertion product (CH_3–MCN). The energies are basically consistent with the identified products (each system produces the most stable products). The observed products also reveal fast conversions between the species including H migration from C to M to reach the energy minima in the reaction path. The conversions to the higher oxidation-state complexes are evidently accompanied by system crossing to the lower multiplicity ground states.

Nevertheless, the absence of the cyanide products (CH_3–MCN, CH_2=M(H)CN, and HC≡$M(H)_2CN$) is a lasting question [27]. They are energetically comparable with the isocyanide counterparts, for example, CH_3–MoCN, CH_2=Mo(H)CN, and HC≡$Mo(H)_2CN$ are 112, 54, and 45 kJ/mol more stable than the reactants. The initial reaction steps (N-coordination to M and formation of the π-complex) are expected to be the same as shown in reaction (2). The strongest CH_3 rocking bands of the cyanide insertion complexes (CH_3–MCN) would appear in the 580–550 cm^{-1} region, where no such absorptions are observed in this study. Their C–N stretching bands expected in the 2120–2170 cm^{-1} region are not observed as well.

$$\begin{aligned} &M + CH_3CN \rightarrow M \leftarrow NCCH_3 \rightarrow \eta^2\text{–}M(NC)\text{–}CH_3 \\ &\quad \rightarrow CH_3\text{–}MCN \rightarrow CH_2{=}M(H)CN \rightarrow HC{\equiv}M(H)_2CN \end{aligned} \tag{2}$$

However, the possibility for formation of the cyanide products still cannot be ruled out due to the relatively lower intensities of their C–N stretching and CH_3 rocking absorptions. Particularly the C–N stretching band, which is normally strong in many other cyanide compounds, is remarkably weak in these cyanide complexes. For example, the C–N stretching band of CH_3–MoCN is fifty times weaker than the N–C stretching band of CH_3–MoNC. In these complexes, the C–N and N–C stretching modes are incorporated with the neighboring M–C and M–N stretching modes, essentially making them to the M–C–N and M–N–C antisymmetric stretching modes. Due to the electron-rich N: center, the polarizations of the M–C and CN bonds of CH_3–MCN are in the same direction whereas those of the M–N and N–C bond of CH_3–MNC in the opposite direction. Therefore, the dipole moment changes of the M–C and CN bonds in CH_3–MCN cancel each other, leading to a weak absorption, whereas those of the M–N and N–C bonds in CH_3–MNC are added resulting in a strong absorption.

3.5. *Molecular structures*

Figs. 10–12 illustrate calculated structures for the M←$NCCH_3$, η^2–M(NC)–CH_3, CH_3–MNC, CH_2=M(H)NC, and HC≡$M(H)_2NC$ products (M = Cr, Mo, and W). While the Cr, Mo, and W N-coordination complexes (M←$NCCH_3$) have near C_s, C_s, and C_{3v} structures in their ground septet, septet, and quintet states, DFT computations started with symmetry constraints overcome the restriction in the first step of geometry optimization. The N-coordinated complex carries a linear M–N–C–C backbone in the quintet state with the shortest N–M bond among the plausible complexes, whereas it is bent in the septet state with the longest N–M bonds, reflecting weak coordination. It is also notable that the multiplicities of these Cr and Mo N-coordination complexes in the ground states are high. We compare computed structures for the weak Cr←$NCCH_3$ complex in Fig. S3 first using B3LYP and the all-electron basis sets 6-311++(3df,3pd) and DZVP, which find 31 and 38 cm^{-1} imaginary CrNC bending frequencies involving the weak Cr–N interaction and second using BPW91 and MP2 with the 6-311++(3df,3pd) set, which find all real frequencies. The problem here is in describing the weak Cr–N interaction, as the $NCCH_3$ subunit dimensions change little in these four calculations.

The C–N bonds of the η^2–M(NC)–CH_3 complexes are shorter than those of the Group 4 and 5 analogs. For example, the C–N bond length 1.242 Å for η^2–Mo(NC)–CH_3 is compared with 1.280 Å for the Zr analog and 1.269 Å for the Nb analog [13,14]. The binding energy also decreases in the order of Zr, Nb, and Mo (189, 148, 55 kJ/mol). This reconfirms the previous conclusion that the extent of back-donation from the metal atom to the π^*-orbital of the coordinated double bond decreases with moving right from the exceptionally strong Group 4 case [11a,13].

The Mo and W isocyanide methylidenes are apparently more agostic than the Group 4 and 5 analogs [13,14]. The smallest metal containing conjugate system has a highly distorted CH_2 group, and the distortion increases with moving right in the same row. The H–C–M bond angles of Zr, Nb, and Mo are 91.3, 90.0, and 86.4° in line with the increasing electronegativities of 1.4, 1.6, and 1.8 for the transition-metals [28]. Similar to the case of Group 4 and 5 metals, the extent of distortion is, however, comparable to those of CH_2=MHX (X = halogen) [6], for example, the agostic angles of 84.6 and 85.3° for CH_2=Mo(H)F and CH_2=Mo(H)Cl. Figs. 10–12 also show that the Group 6 metal methylidynes have C_s structures, which resemble those of HC≡MH_2X investigated in this laboratory [6a]. The contribution of conjugation effects in C=M–N≡C: to the molecular structures are apparently minor, parallel to the cases of Group 4 and 5 metals [13,14].

4. Conclusions

Several products from reactions of laser-ablated Group 6 metal atoms with acetonitrile are observed in the matrix IR spectra. Cr←$NCCH_3$, η^2–Cr(NC)–CH_3, and CH_3–CrNC are identified in the Cr spectra, Mo←$NCCH_3$, η^2–Mo(NC)–CH_3, CH_3–MoNC, and CH_2=Mo(H)NC in the Mo spectra, and HC≡$W(H)_2NC$ provisionally in the W spectra. These products are steps in the reaction path proposed for reactions of Group 4 and 5 metals with acetonitrile [13,14]. They also reconfirm the general tendency that higher oxidation-state complexes are favored with increasing atomic number of the Group 6 metal. The observed Cr and Mo N-coordination complexes suggest that the acetonitrile reaction initiates with coordination with the N-end to the metal atom, similar to the previous observations in acetonitrile solutions and adducts [2,3].

The identified products including the isocyanide complexes indicate that the preferential binding between N and M remains in the reaction course. The observed Cr and Mo N-coordination complexes are bent and carry a weak M–N bond in the septet ground state. The relatively short CN bond in the Group 6 π-complex reveals that the back-donation of the metal atom to the C–N π^* orbital is weaker than in the Group 4 and 5 metal analogs. The Mo and W methylidenes are more agostic than the Group 4 and 5 analogs, parallel to the previously studied methylidene halides [6], and the extents of distortion are also comparable. The methylidyne isocyanide (HC≡$W(H)_2NC$) has a C_s structure similar to HC≡$W(H)_2X$ [6a].

This combined computational and experimental investigation of Group 6 metal atom reactions with acetonitrile clearly benefits from the close working relationship between these two complementary scientific methods.

Acknowledgments

We gratefully acknowledge financial support from National Science Foundation (U.S.) Grant CHE 03-52487 to L.A., and support from the Korea Research Foundation (KRF) grant funded by the Korean government (MEST) (No 2010-0016527).

Appendix. Supplementary data

Supplementary data related to this article can be found online at doi:10.1016/j.jorganchem.2011.12.007.

References

[1] (a) P. Sassi, G. Paliani, R.S. Cataliotti, J. Chem. Phys. 108 (1998) 10197;
(b) S.G. Kukolich, J. Chem. Phys. 76 (1982) 997;
(c) S.T. Sandholm, E. Bjarnov, R.H. Schwendeman, J. Mol. Spectrosc. 95 (1982) 276;
(d) H.S. Mueller, B.J. Drouin, J.C. Pearson, Astron. Astrophys. 506 (2009) 1487.

[2] (a) K.F. Purcell, R.S. Drago, J. Am. Chem. Soc. 88 (1966) 919;
(b) N.R. Brooks, W.A. Henderson, W.H. Smyrl, Acta Cryst. E58 (2002) m176;
(c) R.G. Kidd, H.G. Spinney, Inorg. Chem. 12 (1973) 1967;
(d) A.C. Legon, D.G. Lister, H.E. Warner, J. Am. Chem. Soc. 114 (1992) 8177 (CH_3CN adducts).

[3] (a) K. Balasubrahmanyam, G.J. Janz, J. Am. Chem. Soc. 92 (1970) 4189;
(b) D. Jamrós, M. Wójcik, J. Lindgren, J. Stangret, J. Phys. Chem. B 101 (1997) 6758;
(c) J.-N. Cha, B.-S. Cheong, H.-G. Cho, J. Phys. Chem. A 105 (2001) 1789 (solvation in CH_3CN).

[4] (a) M.E. Jacox, Chem. Phys. 43 (1979) 157;
(b) X. Yang, S. Maeda, K. Ohno, J. Phys. Chem. A 109 (2005) 7319 (Photolysis of CH_3CN);
(c) R. Hattori, E. Suzuki, K. Shimizu, J. Mol. Struct. 738 (2005) 165 (CH_3NC).

[5] (a) G. Maier, C. Schmidt, H.P. Reisenauer, E. Endlein, D. Becker, J. Eckwert, B.A. Hess, L.J. Schaad, Chem. Ber. 126 (1993) 2337;
(b) R. Deng, M. Trenary, J. Phys. Chem. C 111 (2007) 17088 (MeCN isomers).

[6] (a) L. Andrews, H.-G. Cho, Organometallics 25 (2006) 4040 and references therein (Review article, Groups 4–6);
J.T. Lyon, H.-G. Cho, L. Andrews, Organometallics 26 (2007) 2519 (Ti, Zr, Hf + CHX_3, CX_4);
(c) J.T. Lyon, H.-G. Cho, L. Andrews, Organometallics 26 (2007) 6373 (Cr, Mo, W + CHX_3, CX_4);
(d) H.-G. Cho, L. Andrews, J. Phys. Chem. A 110 (2006) 10063 (Group 5 + CH_3X).

[7] (a) H.-G. Cho, L. Andrews, J. Phys. Chem. A 111 (2007) 2480;
(b) H.-G. Cho, L. Andrews, Organometallics 26 (2007) 633 (Group 3 + CH_3X);
(c) H.-G. Cho, L. Andrews, Organometallics 26 (2007) 4096;
(d) H.-G. Cho, L. Andrews, Inorg. Chem. 47 (2008) 1653 (Group 7 + CH_3X).

[8] (a) H.-G. Cho, L. Andrews, Dalton Trans. (2009) 5858;
(b) H.-G. Cho, L. Andrews, Organometallics 27 (2008) 1786 (Group 8 + CH_3X);
(c) H.-G. Cho, L. Andrews, Organometallics 29 (2010) 2211;
(d) H.-G. Cho, L. Andrews, Dalton Trans. 39 (2010) 5478 (Group 9 + CH_3X).

[9] (a) H.-G. Cho, L. Andrews, J. Am. Chem. Soc. 130 (2008) 15836;
(b) H.-G. Cho, L. Andrews, J. Phys. Chem. A 112 (2008) 12293;
(c) H.-G. Cho, L. Andrews, Organometallics 28 (2009) 1358;
(d) H.-G. Cho, L. Andrews, B. Vlaisavljevich, L. Gagliardi, Organometallics 28 (2009) 5623 (Group 10 + CH_3X);
(e) H.-G. Cho, L. Andrews, Dalton Trans. 40 (2011) 11115 (Group 11 + CH_4).

[10] (a) L. Andrews, H.-G. Cho, J. Phys. Chem. A 109 (2005) 6796;
(b) H.-G. Cho, J.T. Lyon, L. Andrews, J. Phys. Chem. A 112 (2008) 6902;
(c) J.T. Lyon, H.-G. Cho, L. Andrews, Eur. J. Inorg. Chem. (2008) 1047 (Actinides + CH_3X);
(d) M.Y. Chen, D.A. Dixon, X.F. Wang, H.-G. Cho, L. Andrews, J. Phys. Chem. A 115 (2011) 5609 (Lanthanides + CH_3X).

[11] (a) H.-G. Cho, G.P. Kushto, L. Andrews, C.W. Bauschlicher Jr., J. Phys. Chem. A 112 (2008) 6295;
(b) P.E.M. Siegbahn, M.R.A. Blomberg, M. Svensson, J. Am. Chem. Soc. 115 (1993) 1952;
(c) M.E. Alikhani, Y. Hannachi, L. Manceron, Y. Bouteiller, Chem. Phys. 103 (1995) 10128;
(d) H.-G. Cho, L. Andrews, J. Phys. Chem. A 112 (2008) 12071;
(e) H.-G. Cho, L. Andrews, J. Phys. Chem. A 111 (2007) 5201 (π- and cyclic complexes).

[12] (a) G. von Frantzius, R. Streubel, K. Brandhorst, J. Grunenberg, Organometallics 25 (2006) 118 and references therein;
(b) N. Berkaine, P. Reinhardt, M.E. Alikhani, Chem. Phys. 343 (2008) 241;
(c) B.O. Roos, R. Lindh, H.-G. Cho, L. Andrews, J. Phys. Chem. A 111 (2007) 6420;
(d) E. Clot, O. Eisenstein, in: N. Kaltzoyannis, J.E. McGrady (Eds.), Computational Inorganic Chemistry, Structure and Bonding, Springer, Heidelberg, 2004, pp. 1–36;
(e) C. Aubert, O. Buisine, M. Malacria, Chem. Rev. 102 (2002) 813 and references therein. (agostic structures).

[13] H.-G. Cho, L. Andrews, J. Phys. Chem. A 114 (2010) 891 (Zr + CH_3CN).

[14] H.-G. Cho, L. Andrews, J. Phys. Chem. A 114 (2010) 5997 (Group 5 + CH_3CN).

[15] L. Andrews, Chem. Soc. Rev. 33 (2004) 123 and references therein.

[16] (a) M.J. Frisch, G.W. Trucks, H.B. Schlegel, G.E. Scuseria, M.A. Robb, J.R. Cheeseman, G. Scalmani, V. Barone, B. Mennucci, G.A. Petersson, H. Nakatsuji, M. Caricato, X. Li, H.P. Hratchian, A.F. Izmaylov, J. Bloino, G. Zheng, J.L. Sonnenberg, M. Hada, M. Ehara, K. Toyota, R. Fukuda, J. Hasegawa, M. Ishida, T. Nakajima, Y. Honda, O. Kitao, H. Nakai, T. Vreven, J.A. Montgomery Jr., J.E. Peralta, F. Ogliaro, M. Bearpark, J.J. Heyd, E. Brothers, K.N. Kudin, V.N. Staroverov, R. Kobayashi, J. Normand, K. Raghavachari, A. Rendell, J.C. Burant, S.S. Iyengar, J. Tomasi, M. Cossi, N. Rega, J.M. Millam, M. Klene, J.E. Knox, J.B. Cross, V. Bakken, C. Adamo, J. Jaramillo, R. Gomperts, R.E. Stratmann, O. Yazyev, A.J. Austin, R. Cammi, C. Pomelli, J.W. Ochterski, R.L. Martin, K. Morokuma, V.G. Zakrzewski, G.A. Voth, P. Salvador, J.J. Dannenberg, S. Dapprich, A.D. Daniels, O. Farkas, J.B. Foresman, J.V. Ortiz, J. Cioslowski, D.J. Fox, Gaussian 09, Revision A.02, Gaussian, Inc., Wallingford, CT, 2009;
(b) N. Godbout, D.R. Salahub, J. Andzelm, E. Wimmer, Can. J. Chem. 70 (1992) 560;
(c) C. Sosa, J. Andzelm, B.C. Elkin, E. Wimmer, K.D. Dobbs, D.A. Dixon, J. Phys. Chem. 96 (1992) 6630;
(d) M. Head-Gordon, J.A. Pople, M.J. Frisch, Chem. Phys. Lett. 153 (1988) 503.

[17] (a) A.D. Becke, J. Chem. Phys. 98 (1993) 5648;
(b) C. Lee, Y. Yang, R.G. Parr, Phys. Rev. B 37 (1988) 785.

[18] K. Raghavachari, G.W. Trucks, J. Chem. Phys. 91 (1989) 1062.

[19] D. Andrae, U. Haeussermann, M. Dolg, H. Stoll, H. Preuss, Theor. Chim. Acta 77 (1990) 123.

[20] (a) A.D. Becke, Phys. Rev. A 38 (1988) 3098;
(b) K. Burke, J.P. Perdew, Y. Wang, in: J.F. Dobson, G. Vignale, M.P. Das (Eds.), Electronic Density Functional Theory: Recent Progress and New Directions, Plenum, 1998;
(c) D.G. Truhlar, Y. Zhao, Acc. Chem. Res. 41 (2008) 157.

[21] (a) A.P. Scott, L. Radom, J. Phys. Chem. 100 (1996) 16502;
(b) M.P. Andersson, P.L. Uvdal, J. Phys. Chem. A 109 (2005) 2937;
(c) C.F. Leypold, M. Reiher, G. Brehm, M.O. Schmitt, S. Schneider, P. Matousek, M. Towrie, Phys. Chem. Chem. Phys. 5 (2003) 1149;
(d) J. Neugebauer, B.A. Hess, J. Chem. Phys. 118 (2003) 7215.

[22] T. Shimanouchi, Tables of Molecular Vibrational Frequencies Consolidated, vol. 1, National Bureau of Standards, 1972, pp. 1–60.

[23] (a) J.J. Garcia, N.M. Brunkan, W.D. Jones, J. Am. Chem. Soc. 124 (2002) 9547;
(b) G. Favero, A. Morvillo, A. Turco, J. Organomet. Chem. 241 (1983) 251 (CN π-complex).

[24] G. Maier, H.P. Reisenauer, K. Rademacher, Chem. Eur. J. 4 (1998) 1957.

[25] X. Wang, L. Andrews, J. Phys. Chem. A 109 (2005) 9021.

[26] (a) X. Wang, L. Andrews, J. Phys. Chem. A 106 (2002) 6720;
(b) X. Wang, L. Andrews, J. Am. Chem. Soc. 124 (2002) 5636.

[27] (a) S. Petrie, Phys. Chem. Chem. Phys. 1 (1999) 2897;
(b) V.M. Rayón, P. Redondo, H. Valdés, C. Barrientos, A. Largo, J. Phys. Chem. A 111 (2007) 6334;
(c) Z.A. Kafafi, R.H. Hauge, J.L. Margrave, Polyhedron 2 (1983) 167 (M(CN) isomerism).

[28] L. Pauling, J. Am. Chem. Soc. 54 (1932) 3570.